Ceramics International 43 (2017) 13185–13192

Contents lists available at ScienceDirect

Ceramics International

journal homepage: www.elsevier.com/locate/ceramint

Liquid flame spray fabrication of WO_3-reduced graphene oxide nanocomposites for enhanced O_3-sensing performances

Yi Liu, Jing Huang, Yongfeng Gong, Xiaomin Xu, Hua Li*

Key Laboratory of Marine Materials and Related Technologies, Zhejiang Key Laboratory of Marine Materials and Protective Technologies, Ningbo Institute of Materials Technology and Engineering, Chinese Academy of Sciences, Ningbo 315201, China

ARTICLE INFO

Keywords:
WO_3-graphene composites
Liquid precursor flame spray
Nanostructure
Ozone sensing

ABSTRACT

WO_3 is one of the inspiring sensing materials that show high response to O_3; an efficient fabrication of WO_3 film with incorporation of complementary additives is essential for enhanced sensitivity. Here we report film deposition by liquid flame spraying, characterization of nanostructured WO_3-reduced graphene oxide (rGO) composites and their gas-sensing activities to O_3. The starting feedstock was prepared from WCl_6 and rGO for pyrolysis synthesis by flame spraying. Nano-porous WO_3-rGO films were successfully fabricated and characterized by transmission electron microscopy, field emission scanning electron microscopy, Raman spectrometry, thermal analyses and X-ray diffraction. Nanosized WO_3 grains exhibited oriented nucleation on rGO flakes whereas rGO retained intact its nano-structural features after spraying. Constrained grain growth of WO_3 of 60–70 nm in size was realized in the rGO-containing films with as compared to ~220 nm in the pure WO_3 film. The WO_3-rGO film sensors showed quicker response to O_3 and faster recovery than rGO-free WO_3 film sensors. Addition of rGO in 1.0 wt% or 3.0 wt% in the films caused a significantly reduced effective working temperature of the film sensors from ~ 250 °C to ~ 150 °C.

1. Introduction

Ozone generator-related air purifiers like ionic and electrostatic air cleaners with ozone as a byproduct have been developed for normal daily use, medical therapy and industrial applications [1,2]. Ozone gas is irritating and toxic even under low concentration levels like several parts per million (ppm). In many cases there have been increasing demands for ozone sensors for possibly controlling the gas emission. Among the existing gas sensors, semiconducting metal oxides were successfully developed for sensing a variety of gases and vapors. Gas-sensing activities of some metal oxides such as tungsten trioxide (WO_3) [3–6], tin oxide (SnO_2) [7], zinc oxide (ZnO) [8], titanium dioxide (TiO_2) [9], indium sesquioxide (In_2O_3) [10] and molybdenum oxide (MoO_3) [11] have been evidenced effective for sensing many pollutant components of atmosphere. The detection mechanisms of the semiconductor-based sensors are related to the phenomenon that adsorption or desorption of target gas on the metal oxide surface changes its conductivity. Challenges persist yet pertaining to developing appropriate technical routes for making the semiconductor films for long-term functional services.

WO_3 is an important n-type metal oxide semiconductor with oxygen vacancies, which act as donors and exhibit high sensitivity particularly to ozone. Taking into account its small band gap (2.585 ev) and stable physicochemical properties, nanostructured WO_3 is generally considered as a competitive candidate material for chemical sensors. Its sensitivity to target gas can be as low as parts per billion (ppb). WO3-based sensor was already attempted to monitor oxidizing inorganic gases (for instance O_3 [3–5], NO_2 [12], and SO_2 [13]), reducing inorganic gases (for instance H_2S [6], H_2 [14], NO [12], CO [15] and NH_3 [6]), and organic vapors (for instance acetone [6], ethanol [6]). To further enhance the sensitivity of WO_3 sensors, recent research efforts have been devoted to constructing high surface areas [6,16–18] and incorporating appropriate additives to attain nanocomposite structures [19–21].

Among the additives that have been investigated, metals such as silver [13], platinum [14], gold [19], palladium [20], or chromium [21] are catalysts that promote chemical reactions by reducing the activation energy between sensor and target gas, enhancing the receptor function which further promotes the selectivity and sensitivity of the sensors. As one of the most exciting materials, graphene is a fascinating material for sensing due to its large specific surface area for molecular adsorption and outstanding electrical properties such as low noise level and high carrier mobility [22–24]. Detection of gases by graphene is predominately attributed to its conductance changes upon the adsorp-

* Corresponding author.
E-mail address: lihua@nimte.ac.cn (H. Li).

http://dx.doi.org/10.1016/j.ceramint.2017.07.012
Received 6 January 2017; Received in revised form 3 June 2017; Accepted 2 July 2017
Available online 03 July 2017
0272-8842/

tion of sensed species. Extremely high carrier mobility of graphene at room temperature indicates that graphene is a promising candidate for low temperature gas sensing.

To date, many techniques such as dip coating method [25], sol-gel processing [9], electron-beam evaporation [26], pulsed laser deposition [27], magnetron sputter deposition [28], hydrothermal synthesis [29] and spinning coating method [29,30] have been tried to make sensor films. Regardless of the encouraging sensing performances of the sensors, it must be noted that these technical routes for fabricating the semiconductor films still have difficulties in large-scale construction of controllable nanostructures. As one of the most extensively applied surface coating techniques, thermal spray already showed promises in producing WO_3 films with exciting gas-sensing performances [31–33]. Our previous work already revealed that compared to traditional thermal spray processes, liquid flame spray seemed to be more appropriate for depositing sufficiently stable porous network-like structure in WO_3 film. Involvement of liquid in the spraying gives rise to sintering of the WO_3 nano-particles for enhanced particle interconnectivity, yet with well-retained high specific surface area. In this work, we further fabricated WO_3-reduced graphene oxide (rGO) films by liquid flame spray. Graphene was selected as the complementary additives with an aim of achieving remarkably enhanced sensing capability of WO_3 films. Spray pyrolysis was made during the flame spray processing for synthesizing WO_3 and microstructure of the films was characterized. The ozone-sensing performances of the films were examined and elucidated, giving clear insight into flame spray fabrication of the novel nanocomposites for gas-sensing applications.

2. Materials and methods

2.1. Synthesis of graphene and WO_3-rGO composites

Reduced graphite oxide was chemically synthesized from high purity flakey graphite. Graphite oxide was prepared by oxidation and exfoliation of graphite via the modified Hummer's method [34,35]. Reduction of graphite oxide was subsequently carried out by thermal reduction processing at 200 °C for 30 min. The detailed procedures and microstructure characterization have been reported previously [36,37]. Tungsten chloride (WCl_6) (Aladdin Reagent Corporation, China) was used for pyrolysis synthesis of tungsten trioxide (WO_3) by flame spraying. For fabrication of the WO_3-rGO nanocomposites, the as-received rGO was ultrasonically dispersed in 250 ml ethanol solution for 2 h with the ultrasound power of 360 W. 25 g WCl_6 was added into the as-obtained rGO solution, followed by slowly adding 250 ml deionized water solution containing 0.4 g polyethylene glycol (PEG, Sino Pharm Chemical Reagent Co. Ltd, China). The resultant suspension was mechanically stirred for 1 h. WO_3-rGO composite precursor solutions with different content of rGO (0 wt%, 1.0 wt%, and 3.0 wt%) were typically prepared. Previous preliminary study showed that further increased content of rGO, for example 4.0 wt% or 5.0 wt%, in the solution already brought about difficulties in making their films, and remarkably low deposition efficiency was encountered. The preparation procedure is schematically shown in Fig. 1a.

2.2. Fabrication of WO_3-rGO films

Gold electrodes were printed by screen printing method and sintered on alumina substrate. The WO_3-rGO films were deposited by liquid flame spray on the substrate with the dimension of 30 × 20 × 1 mm in length, width, and thickness respectively (Fig. 1b). During the deposition, the precursor was fed vertically into the flame. The liquid flame deposition was carried out using the CDS 8000 system (Castolin, Germany). Oxygen and acetylene were used as the combustion-supporting gas and the fuel gas with the pressure of 0.7 MPa and 0.1 MPa, respectively. Feeding rate of the solution feedstock was 40 ml/min and the spray distance was 200 mm.

2.3. Characterization of microstructure

Microstructure of the powder and the films was characterized by transmission electron microscopy (TEM, FEI Tecnai F20, the Netherlands) and field emission scanning electron microscopy (FESEM, FEI Quanta FEG250, the Netherlands). For the TEM characterization, specimen preparation involved transferring the precursors onto the micro grids and letting the solvent evaporate. Phase composition of the samples was analyzed by X-ray diffraction (XRD, D8 Advance, Bruker AXS, Germany) using CuKα radiation (λ = 1.5406 Å) operated at 40 kV and 40 mA. The goniometer was set at a scan rate of 0.033°/s over a 2θ range of 20–35°. rGO dispersed in WO_3 matrix was characterized by Raman spectroscopy (Renishaw inVia Reflex, Renishaw, UK). The Diamond TG/DTA system (PerkinElmer, USA) was used to carry out the thermogravimetric analysis (TGA) of the samples in air with the heating rate of 10 °C/min.

2.4. Assessment of O_3 sensing properties

Gas-sensing capability of the coated sensors was examined by measuring their response to ozone gas in a Teflon chamber. The sensors were connected to a tailor-made system to acquire the electrical resistance and to control their temperature during the testing. Dry air and ozone gas were introduced into the tube alternatively. Ozone gas was generated by a FL-8F ozone generator (Feili Ltd., China). Concentration of the ozone gas in the testing system was adjusted from 0.5 to 10.0 ppm and calibrated by an ozone detector (HJ-BXA-O_3, Huijin Tech Ltd., China). The sensors were heated to different working temperatures of 100–300 °C by controlling the electrical voltage of the Pt heater. The sensor responses for the gas (O_3 in air) were measured (Fig. 1b), which were determined by: $S = \frac{R_{gas} - R_{air}}{R_{air}}$, where R_{gas} and R_{air} denote the resistance of the as-deposited film in the environment of gas mixture and air, respectively. The response performances of the sensors was measured by the transient time to the steady-state

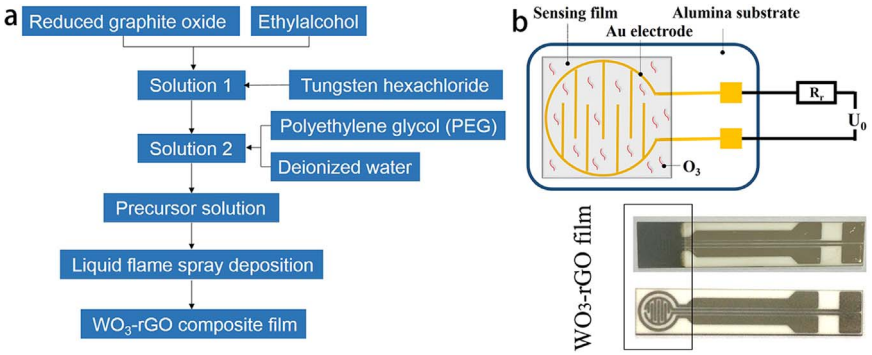

Fig. 1. Processing flow chart for the film fabrication (a), and schematic depiction of the basic circuit for the WO_3-rGO coated sensor (b).

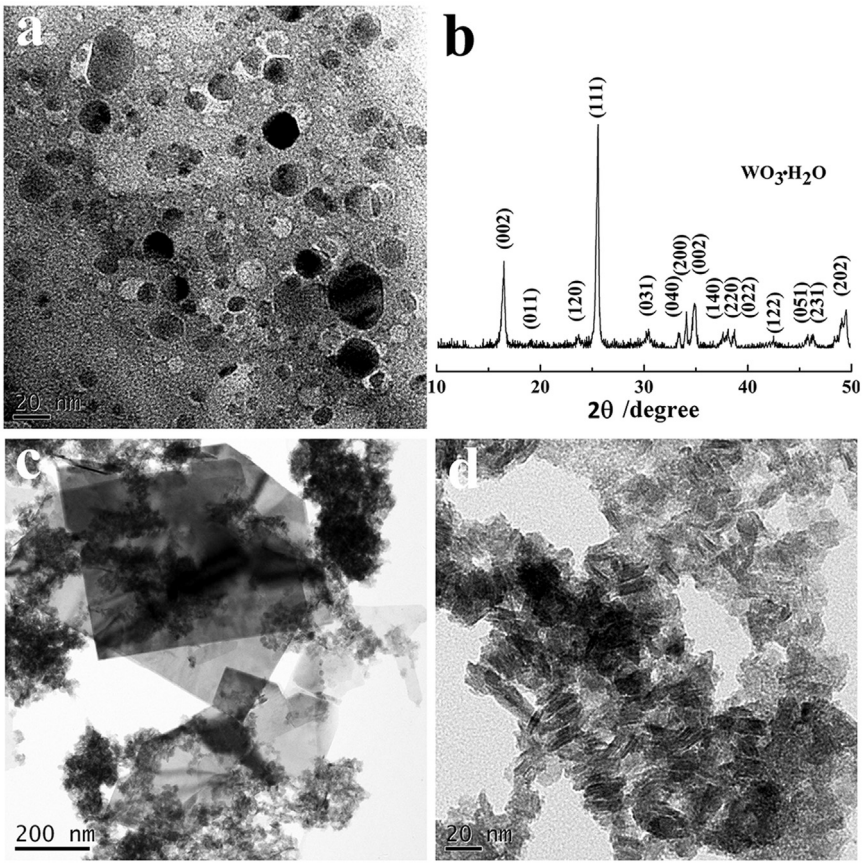

Fig. 2. Characteristics of the WO_3 precursor (a, b) and the WO_3-rGO precursor (c, d), (a) TEM image of the pure WO_3 precursor showing $WO_3 \cdot H_2O$ grains, (b) XRD pattern of the WO_3 precursor showing sole component of $WO_3 \cdot H_2O$, (c) TEM image of the WO_3-rGO precursor showing wrinkled paper-like morphology of rGO and adhered $WO_3 \cdot H_2O$ nano grains on rGO flakes, and (d) enlarged TEM image of the rod-like $WO_3 \cdot H_2O$ nano grains in the rGO-containing precursor.

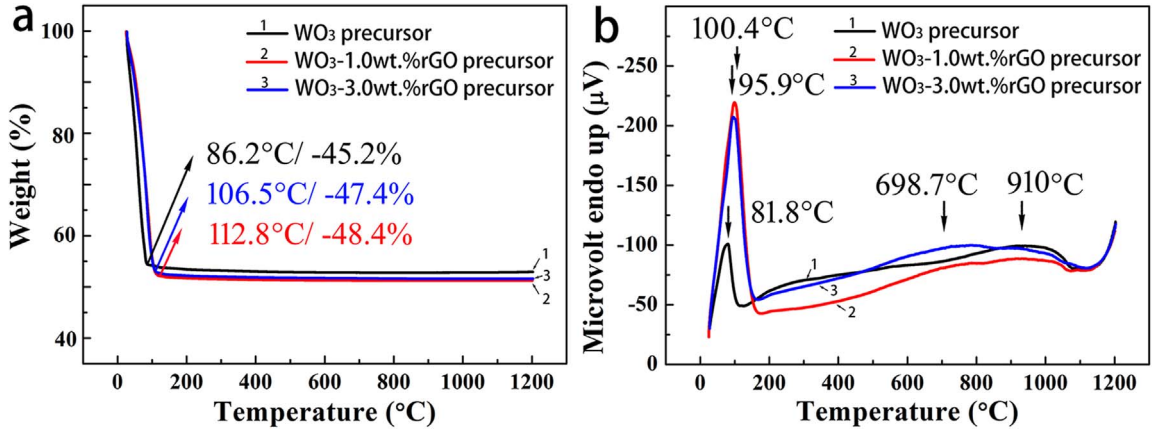

Fig. 3. TG curves (a) and TGA curves of the WO_3 and the WO_3-rGO precursors.

resistance upon their exposure to O_3. Response time and recovery time were defined as the time for the sensors to attain 90% change due to chemical adsorption.

3. Results and discussion

TEM image of the precursor synthesized via the chemical approach without addition of rGO shows well-dispersed nanosized WO_3 particles (Fig. 2a). The tungsten oxide grains have the size of 8–50 nm. XRD curves of tungsten oxide precursor match with $WO_3 \cdot H_2O$ (JCPDS No. 84-0886) (Fig. 2b). As the amount of water in mixed solvent increases, mole fraction of oxygen in the tungsten oxide system also increases, which is likely due to the fact that water is the source of oxygen for the solvothermal synthesis [38]. The dried products of the precursor at room temperature show no trace of WO_3, indicating clearly that heat source is essential for WO_3 synthesis from the solution precursor and in fact monoclinic WO_3 was successfully synthesized during the spraying.

The as-received rGO shows wrinkled paper-like morphology and some other characteristics were described in our previously published papers [36,37]. TEM observation revealed that $WO_3 \cdot H_2O$ nanograins intimately attach to rGO flakes (Fig. 2c). Close view demonstrates rod-like particles in the rGO-containing precursor (Fig. 2d). $WO_3 \cdot H_2O$ grains have the size of 20 nm in length and 5 nm in diameter, thereby

implying preferred crystallographic orientation of WO_3 growth induced by rGO sheets.

During the liquid flame spraying of the WO_3-rGO precursor, liquid droplets injected into the flame are subjected to a maximum temperature of 2600 °C and are accelerated to about 160 ms^{-1} [39]. Thermal analyses were therefore carried out to examine the behaviors of WO_3 phase during high temperature processing (Fig. 3). DTA and TG measurements were made in static air from room temperature to 1200 °C. It is noted that there is an obvious weight loss (as indicated by the TG curve, Fig. 3a) and a strong exothermic peak (as suggested by the DTA curve, Fig. 3b) from 80 °C to 110 °C, referring to release of solvent, ethanol molecules and water molecules in this case. Weight loss of the surfactant PEG is not detected due to its low content. In addition, dehydration of $WO_3 \cdot H_2O$ is suggested with the formation of WO_3 below the temperature of 200 °C [38]. The small exothermic DTA peak at 698.7 °C (Fig. 3b) with undetectable weight loss (Fig. 3a) is presumably attributed to combustion of few rGO nansheets. The peak located at ~ 910 °C likely refers to phase transformation of WO_3 [40].

Nanostructured WO_3 and WO_3-rGO films were successfully deposited on alumina substrates by the liquid flame spray processing. Raman and XRD detection reveals the sole presence of monoclinic WO_3 in the films (Fig. 4), indicating complete synthesis of WO_3 during the spraying. Broadened XRD peak of alumina at ~26° of 2θ is seen for the rGO-containing films. This is presumably attributed to grain refining or microstrain broadening of alumina occurred at top surface of the substrate, since prior to the coating deposition, pre-heating of the alumina substrate was made using the flame. In addition, it is noted that rGO is retained after the film deposition (Fig. 4b). rGO is suggested by the G band at 1578 cm^{-1} on the Raman curve (Fig. 4b) [41].

Microstructural characterization reveals interesting morphologies of the films (Fig. 5). Fractured cross-sections show unique film thickness (Fig. 5a), and it is tailorable by changing deposition time. It is noted, however, that addition of rGO reduced the deposition efficiency of the precursors for the film fabrication (Fig. 5c-1, b-1 versus a-1). The films show the thickness of 5 μm, 0.9 μm and 0.6 μm for the pure WO_3, the WO_3-1.0 wt%rGO and the WO_3-3.0 wt%rGO films. It is established that film thickness is critical in deciding diffusivity and reactivity of target gas molecules. Electrical resistance and sensor response of the sensor films to certain gases decreased monotonically with increase in film thickness, while some gases responded almost independently of the film thickness [42]. In this case, thickness, microstructural characteristics, and chemistry of the films might synergistically play roles in regulating their gas-sensing performances. In addition, FESEM views from top surfaces of the films (Fig. 5a-2, b-2 and c-2) suggest remarkably different microstructural features of the films with/without addition of rGO. The pure WO_3 film exhibits more porous network with large pores of ~4 μm (Fig. 5a-2, a-3), while the rGO-containing WO_3 films show meso-/micro- porous topographical feature. rGO sheets are uniformly dispersed in WO_3 matrix (Fig. 5b, c). For macropores with pore size larger than 50 nm, gas transport occurs mainly by molecular diffusion (confinement by the pore boundaries is less significant), whereas for micropores with pore size less than 2 nm, surface diffusion becomes predominant. The transport without external pressure can be described by Knudsen diffusion and the diffusion coefficient $D_k = 4r/3\sqrt{(2RT/\pi M}$ [43], where R is the universal gas constant, M is molecular weight of the gas molecule, and r is pore radius. In theory, larger pores would result in better diffusivity of the target gas, giving rise to higher gas sensitivity of the films.

In fact, gas diffusion is a complex issue reflecting the influence of various structural and textural parameters of sensing films. Grain size and specific surface area of the films are predominately the key factors responsible for their gas sensing performances. For the rGO-containing films, a large number of tiny particles are clearly recognized, which mainly grow on rGO sheets. The particles show a size of ~ 60–70 nm (Fig. 6b), and the pure WO_3 film shows the particle size of ~220 nm (Fig. 6a). These structural features suggest intact state of rGO during the spraying and WO_3 particles opt to adhere on rGO sheets during the film deposition. A schematic depiction is proposed to illustrate the WO_3 formation superimposing on the surface of rGO sheets (Fig. 6c). The flame spray processing enhances nucleation of WO_3 on rGO sheets and, however, the rGO sheets constrain fast growth of the adhered WO_3 grains (60–70 nm versus 220 nm). This could be explained by the inhibited grain growth along at least one direction, that is, the direction perpendicular to the interface between the adhered WO_3 grain and rGO sheet. These specific structures alone might already affect the gas-sensing performances of WO_3. Theoretically, the changes in conductance of sensing materials occur at the exterior regions of their grains. Beyond the depletion layer, interior parts of the grains do not contribute to gas response [44]. As a consequence, grain size affects the sensor performance substantially. Smaller crystal size gives rise to greater sensitivity of the bulk film [8,44,45]. Our results suggest that the addition of rGO increases the specific surface area of WO_3-based films, which could in turn provide more adsorption sites for gas reaction.

To gain clear insight into the impact of the WO_3-rGO composite structure on gas sensing performances, response of the films to O_3 was examined (Fig. 7). As one of the crucial factors that affect the sensing performances, the operation temperature was altered to inspect the response of the films to O_3. Results show that the responses are enhanced and reach the maximum and then decline rapidly with

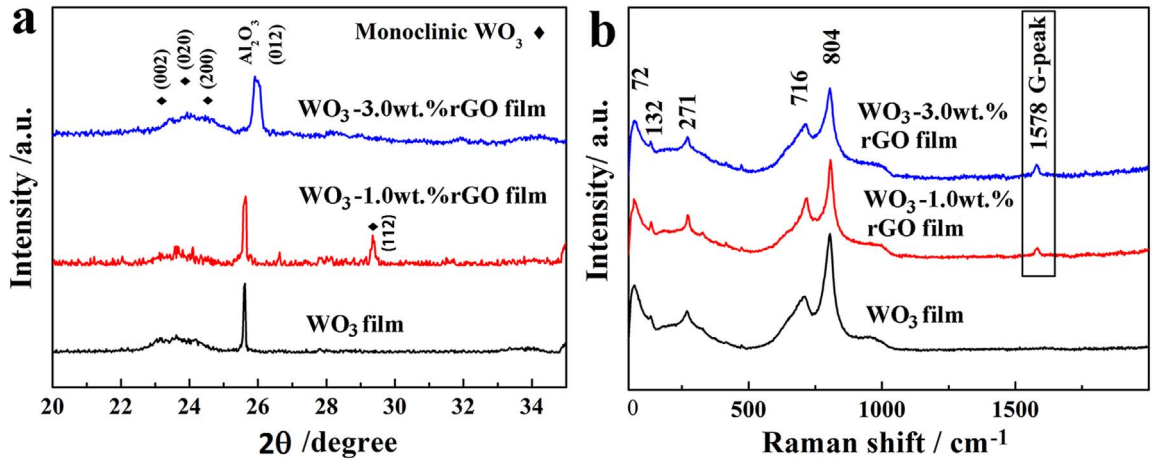

Fig. 4. XRD curves (a) and Raman spectra (b) of the samples (the Al_2O_3 XRD peaks are detected from the substrate).

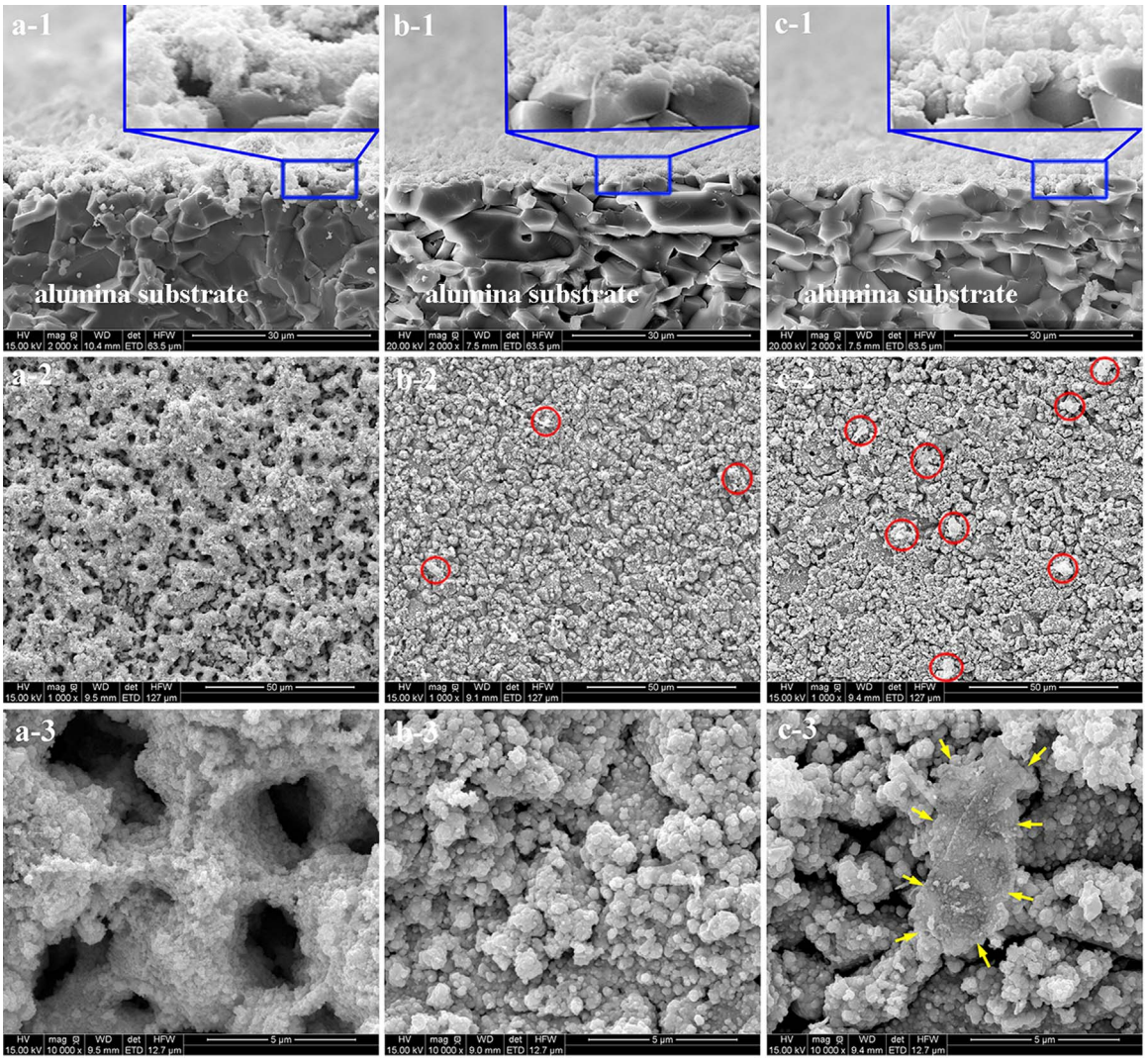

Fig. 5. FESEM views of the as-deposited nanostructured films, (a) the pure WO_3 film, (b) the WO_3-1.0 wt% rGO film, and (c) the WO_3-3.0 wt% rGO film. (–1: cross-sectional view, –2: surface view, and –3: further magnified surface view). The red circles highlight typical rGO existing on the top layer of the films, and the yellow arrows point to rGO sheet). (For interpretation of the references to color in this figure legend, the reader is referred to the web version of this article).

increase in the operation temperature (Fig. 7a). Surprisingly, it is realized that addition of rGO platelets changed the temperature at which point maximum response is attained. The temperature changes from ~ 250 °C for the rGO-free WO_3 films to ~ 150 °C for the rGO-containing WO_3 films. Medium to high working temperature (typically in the range of 200–500 °C) has been the major hurdle for applications of semiconductor-based sensors [3,18,46], since the markedly high operation temperature triggers many obstacle problems, e.g. undesired grain growth [44,45], elongated response time [25], collapsed pore structure, noticeable power consumption, and others, which could either shorten service duration of the sensors or reduce their sensitivity. It is exciting to note that incorporation of rGO effectively reduces the working temperature of the sensor. Compared with previously reported semiconductor-based sensors for ozone detection [25,47], the WO_3-rGO films fabricated by the liquid flame spray route show much lower optimum operation temperature (T_{opt}) and higher sensitivity. The rationale for the necessarily required temperature could lie in the kinetics of both the reactions of target gas molecules with surface-adsorbed oxygen and the replacement of the oxygen from gas molecules. In addition, the working temperature is also essential for facilitating gas diffusion through the sensing layer. The tendency between operation temperature and sensor response is commonly observed and this is believed to be resulted from the competition between slow kinetics at low temperature and enhanced desorption at high temperature [18,43]. For the WO_3-based sensor films, upon their exposure to oxidizing O_3 gas, the gas molecules can easily adsorb on the active sites of the films and capture the electrons from WO_3, in turn enhancing the electron-depletion for increased electrical resistance [3]. For the synthesized rGO in the WO_3-rGO films, there have been considerable structural disorders in graphene lattice [36]. Due to well retained functional groups of rGO in the films, the interaction of gas with rGO is anticipated at the defects [48,49]. In O_3 atmosphere, carbon atoms could be removed from graphene lattice and vacancies are formed which could further enhance the sensing performances [24,48]. In addition, graphene has large surface area with respect to its volume due to its unique two-dimensional structural features. For the rGO-containing films, the large surface area can presumably facilitate O_3 adsorption and diffusion on active surfaces. Moreover, the superior electrical property of rGO and potential barrier (Schottky barrier) at the WO_3/rGO interface could contribute to improved conductivity and specific capture and migration of electrons from WO_3 to rGO [50], leading to a better sensing behavior.

Gas sensing assessment revealed significantly enhanced sensitivity of the rGO-containing WO_3 sensors to ozone (Fig. 7b). The response of the sensor operated at 150 °C is almost proportional to the ozone concentration ranging from 0.5 to 10 ppm. Higher content of rGO in

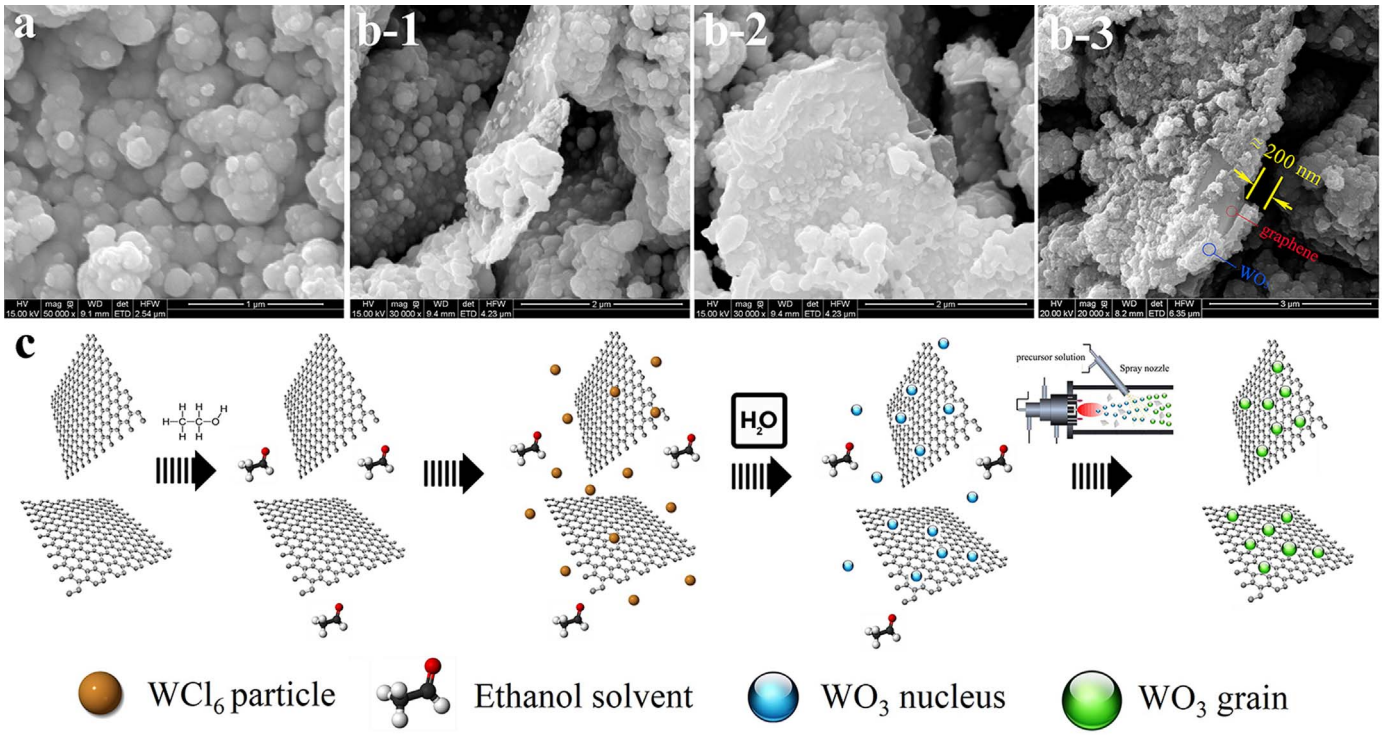

Fig. 6. WO_3 grain growth by rGO sheets in the films and schematic depiction illustrating structure evolvement of the WO_3-rGO composites during the chemical synthesis and liquid flame spray deposition. (a) The pure WO_3 film showing the WO_3 grain size of ~220 nm, (b) SEM image showing WO_3 nanograins adhered to rGO flakes with an intimate contact, (c) cartoon showing formation of the WO_3-rGO nanocomposite structures.

the films gives rise to better sensing response and the WO_3-3.0 wt% rGO sensor has almost 4 times sensing response better than the pure WO_3 sensor. It has been reported WO_3 nanorods/graphene nanocomposites performed high-efficiency visible-light-driven photocatalysis and NO_2 gas sensing [50]. Our finding is consistent with the existing results that graphene promotes the sensing performances of the semiconductor sensors.

In addition, the responses and the recovery responses of the sensors based on the WO_3 film and the WO_3-rGO films were also examined under 10 ppm O_3 tested at 150 °C (Fig. 8). The resistance of the sensors can be recovered to the initial values after they were put back to air. The response time and the recovery time of the WO_3 and the WO_3-1.0 wt%rGO sensors are 64.6 s and 40.6 s, 26.9 s and 29.1 s, respectively. The WO_3-3.0 wt%rGO sensor shows the values of 17.1 s and 32.7 s, respectively, which are remarkably shorter than the time required by other semiconductor-based sensors like ZnO-rGO sensor to NO_2 [46]. The higher sensitivity and quicker response of the rGO-containing WO_3 sensors could be partly attributed to the smaller grain size of WO_3 grains and the higher surface area of the films, which could enhance the adsorption capability for O_3 gas. Part of our ongoing efforts are devoted to exploring the possibilities of fabricating the WO_3-rGO films with higher content of rGO (higher than 3.0 wt%). In addition, the mechanisms as to how the WO_3/rGO interfaces affect the sensing performances are yet to be further elucidated.

4. Conclusions

Nano-porous WO_3-rGO films have been successfully fabricated by liquid flame spraying WCl_6 and rGO precursor. The films showed tailorable thickness and WO_3 grains opted to nucleate on and grew along rGO nanosheets during the spraying. Significantly constrained growth of WO_3 grains was realized in the nanocomposite films and the structural features of rGO were retained after the spraying. Addition of rGO significantly enhanced the sensitivity of the WO_3 films to O_3 and

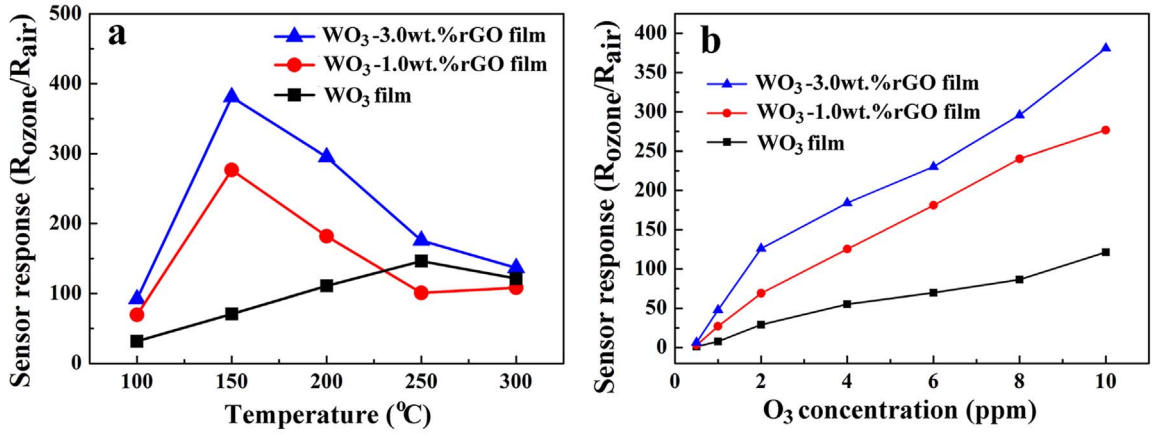

Fig. 7. Sensing performances of the films to O_3, (a) sensitivity versus operation temperature (O_3: 10 ppm), and (b) sensitivity versus O_3 concentration tested at 150 °C.

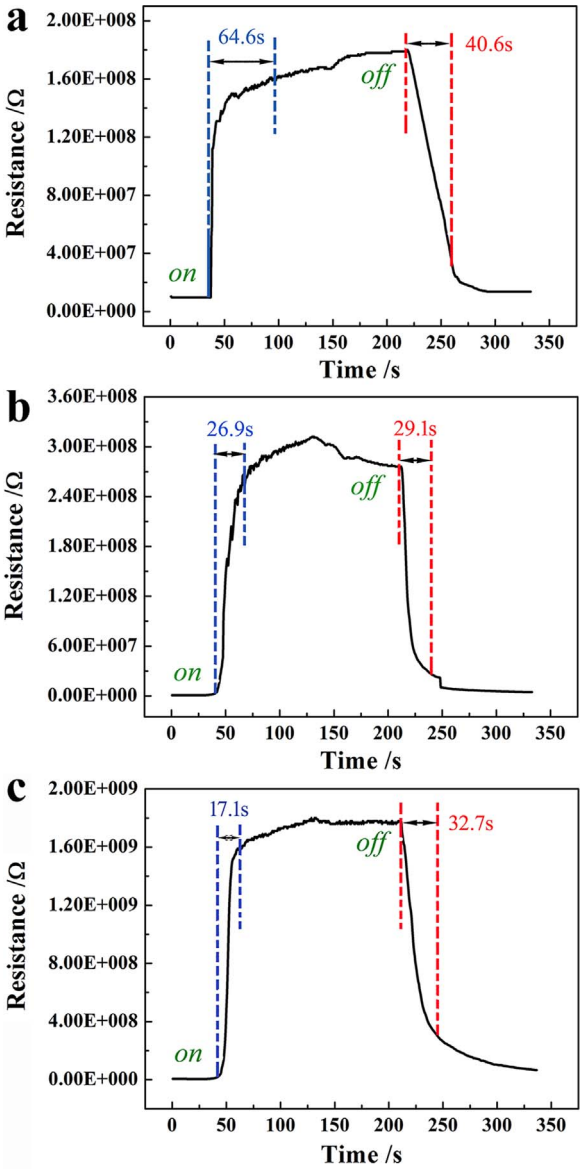

Fig. 8. Response and recovery curves of the WO_3 sensor (a), the WO_3-1.0 wt%rGO sensor (b), and the WO_3-3.0 wt%rGO sensor (c).

reduced the effective working temperature of the sensors from ~ 250 °C to ~ 150 °C. The results would give insight into selection and preparation of new sensing nanomaterials and their film fabrication by liquid flame spray technical route for gas-sensing applications.

Acknowledgements

This work was supported by National Natural Science Foundation of China (grant # 31500772 and 41476064), China Postdoctoral Science Foundation (grant # 2016T90554 and 2014M561800), Key Research and Development Program of Zhejiang Province (grant # 2017C01003), and Ningbo Natural Science Foundation (grant # 2015A610019).

References

[1] B.C. Singer, B.K. Coleman, H. Destaillats, A.T. Hodgson, M.M. Lunden, C.J. Weschler, W.W. Nazaroff, Indoor secondary pollutants from cleaning product and air freshener use in the presence of ozone, Atmos. Environ. 40 (2006) 6696–6710.

[2] N. Britigan, A. Ahmad, A.N. Sergey, Quantification of ozone levels in indoor environments generated by ionization and ozonolysis air purifiers, J. Air Waste Manag. 56 (2006) 601–610.

[3] J. Guérin, K. Aguir, M. Bendahan, C. Lambert-Mauriat, Thermal modelling of a WO_3 ozone sensor response, Sens. Actuators B 104 (2005) 289–293.

[4] J. Guerin, K. Aguir, M. Bendahan, Modeling of the conduction in a WO_3 thin film as ozone sensor, Sens. Actuators B 119 (2006) 327–334.

[5] A. Mirzaei, S.G. Leonardi, G. Neri, Detection of hazardous volatile organic compounds (VOCs) by metal oxide nanostructures-based gas sensors: A review, Ceram. Int. http://dx.doi.org/10.1016/j.ceramint.2016.06.145.

[6] X.L. Li, T.J. Lou, X.M. Sun, Y.D. Li, Highly sensitive WO_3 hollow-sphere gas sensors, Inorg. Chem. 43 (2004) 5442–5449.

[7] G. Korotcenkov, I. Blinov, M. Ivanov, J.R. Stetter, Ozone sensors on the base of SnO_2 films deposited by spray pyrolysis, Sens. Actuators B: Chem. 120 (2007) 679–686.

[8] R. Martins, E. Fortunato, P. Nunes, I. Ferreira, A. Marques, M. Bender, N. Katsarakis, V. Cimalla, G. Kiriakidis, Zinc oxide as an ozone sensor, J. Appl. Phys. 96 (1398) (2004) 1398–1408.

[9] C. Garzella, E. Comini, E. Tempesti, C. Frigeri, G. Sberveglieri, TiO_2 thin films by a novel sol-gel processing for gas sensor applications, Sens. Actuators B 68 (2000) 189–196.

[10] M. Ivanovskaya, A. Gurlo, P. Bogdanov, Mechanism of O_3 and NO_2 detection and selectivity of In_2O_3 sensor, Sens. Actuators B 77 (2001) 264–267.

[11] M. Ferroni, V. Guidi, G. Martinelli, P. Nelli, M. Sacerdoti, G. Sberveglieri, Characterization of a molybdenum oxide sputtered thin film as a gas sensor, Thin Solid Films 307 (1997) 148–151.

[12] M. Akiyama, J. Tamaki, N. Miura, N. Yamazoe, Tungsten oxide-based semiconductor sensor highly sensitive to NO and NO_2, Chem. Lett. (1991) 1611–1614.

[13] Y. Shimizu, N. Matsunaga, T. Hyodo, M. Egashira, Improvement of SO_2 sensing properties of WO_3 by noble metal loading, Sens. Actuators B: Chem. 77 (2001) 35–40.

[14] L.F. Zhu, J.C. She, J.Y. Luo, S.Z. Deng, J. Chen, N.S. Xu, Study of physical and chemical processes of H_2 sensing of Pt-coated WO_3 nanowire films, J. Phys. Chem. C 114 (2010) 15504–15509.

[15] A.M. Azad, M. Hammoud, Fine-tuning of ceramic-based chemical sensors via novel microstructural modification: i: Low level CO sensing by tungsten oxide, WO_3, Sens. Actuators B: Chem. 119 (2006) 384–391.

[16] S.L. Darshane, S.S. Suryavanshi, I.S. Mulla, Nanostructured nickel ferrite: a liquid petroleum gas sensor, Ceram. Int. 35 (2009) 1793–1797.

[17] Y. Shen, T. Yamazaki, Z. Liu, D. Meng, T. Kikuta, N. Nakatani, Influence of effective surface area on gas sensing properties of WO_3 sputtered thin films, Thin Solid Films 517 (2009) 2069–2072.

[18] C. Wang, L. Yin, L. Zhang, D. Xiang, R. Gao, Metal oxide gas sensors: sensitivity and influencing factors, Sensors 10 (2010) 2088–2106.

[19] N. Hongsith, C. Viriyaworasakul, P. Mangkorntong, N. Mangkorntong, S. Choopun, Ethanol sensor based on ZnO and Au-doped ZnO nanowires, Ceram. Int. 34 (2008) 823–826.

[20] A. Esfandiara, A. Irajizada, O. Akhavana, S. Ghasemic, M.R. Gholamic, Pd-WO_3/reduced graphene oxide hierarchical nanostructures as efficient hydrogen gas sensors, Int. J. Hydrog. Energy 39 (2014) 8169–8179.

[21] E. Rossinyol, A. Prim, E. Pellicer, J. Arbiol, F. Hernández-Ramírez, F. Peiró, A. Cornet, J.R. Morante, L.A. Solovyov, B. Tian, T. Bo, D. Zhao, Synthesis and characterization of chromium-doped mesoporous tungsten oxide for gas sensing applications, Adv. Funct. Mater. 17 (2007) 1801–1806.

[22] W.J. Yuan, G.Q. Shi, Graphene-based gas sensors, J. Mater. Chem. A 1 (2013) 10078–10091.

[23] H.J. Yoon, D.H. Jun, J.H. Yang, Z.X. Zhou, S.S. Yang, M.M. Cheng, Carbon dioxide gas sensor using a graphene sheet, Sens. Actuators B 157 (2011) 310–313.

[24] M.G. Chung, D.H. Kim, H.M. Lee, T. Kim, J.H. Choi, D.K. Seo, J.B. Yoo, S.H. Hong, T.J. Kang, Y.H. Kim, Highly sensitive NO_2 gas sensor based on ozone treated graphene, Sens. Actuators B 166–167 (2012) 172–176.

[25] A. Hattori, H. Tachibana, N. Yoshiike, A. Yoshida, Ozone sensor made by dip coating method, Sens. Actuators B 77 (1999) 120–125.

[26] J. Tamaki, C. Naruo, Y. Yamamoto, M. Matsuoka, Sensing properties to dilute chlorine gas of indium oxide based thin film sensors prepared by electron beam evaporation, Sens. Actuators B 83 (2002) 190–194.

[27] E. György, G. Socol, E. Axente, I.N. Mihailescu, C. Ducu, S. Ciuc, Anatase phase TiO_2 thin films obtained by pulsed laser deposition for gas sensing applications, Appl. Surf. Sci. 247 (2005) 429–433.

[28] C. Lemire, D.B.B. Lollman, A. Al Mohammad, E. Gillet, K. Aguir, Reactive R.F. magnetron sputtering deposition of WO_3 thin films, Sens. Actuators B 144 (2010) 280–288.

[29] D.D. Vuong, G. Sakai, K. Shimanoe, N. Yamazoe, Preparation of grain size-controlled tin oxide sols by hydrothermal treatment for thin film sensor application, Sens. Actuators B 103 (2004) 386–391.

[30] H.Y. Bae, G.M. Choi, Electrical and reducing gas sensing properties of ZnO and ZnO-CuO thin films fabricated by spin coating method, Sens. Actuators B 55 (1999) 47–54.

[31] C. Zhang, M. Debliquy, A. Boudiba, H.L. Liao, C. Coddet, Sensing properties of atmospheric plasma-sprayed WO_3 coating for sub-ppm NO_2 detection, Sens. Actuators B 144 (2010) 280–288.

[32] C. Zhang, M. Debliquy, H.L. Liao, Deposition and microstructure characterization of atmospheric plasma-sprayed ZnO coatings for NO_2 detection, Appl. Surf. Sci. 256 (2010) 5905–5910.

[33] Q.F. Wu, J. Huang, H. Li, Deposition of porous nano-WO_3 coatings with tunable grain shapes by liquid plasma spraying for gas-sensing applications, Mater. Lett. 141 (2015) 100–103.

[34] M.J. McAllister, J.L. Li, D.H. Adamson, H.C. Schniepp, A.A. Abdala, J. Liu, M. Herrera-Alonso, D.L. Milius, R. Car, R.K. Prud'homme, I.A. Aksay, Single sheet functionalized graphene by oxidation and thermal expansion of graphite, Chem. Mater. 19 (2007) 4396–4404.

[35] W.S. Hummers Jr, R.E. Offeman, Preparation of graphitic oxide, J. Am. Chem. Soc. 80 (1958) 1339.
[36] Y. Liu, J. Huang, H. Li, Synthesis of hydroxyapatite-reduced graphite oxide composites for biomedical applications: oriented nucleation and epitaxial growth of hydroxyapatite, J. Mater. Chem. B 1 (2013) 1826–1834.
[37] Y. Liu, Z.H. Dang, Y.Y. Wang, J. Huang, H. Li, Hydroxyapatite/graphene-nanosheet composite coatings deposited by vacuum cold spraying for biomedical applications: inherited nanostructures and enhanced properties, Carbon 67 (2014) 250–259.
[38] H.G. Choi, Y.H. Jung, D.K. Kim, Solvothermal synthesis of tungsten oxide nanorod/nanowire/nanosheet, J. Am. Ceram. Soc. 88 (2005) 1684–1686.
[39] J. Tikkanen, K.A. Gross, C.C. Berndt, V. Pitkanen, J. Keskinen, S. Raghu, M. Rajala, J. Karthikeyan, Characteristics of the liquid flame spray process, Surf. Coat. Tech. 90 (1997) 210–216.
[40] E. Salje, K. Viswanathan, Physical properties and phase transitions in WO_3, Acta Cryst. A31 (1975) 356–359.
[41] A.C. Ferrari, J.C. Meyer, V. Scardaci, C. Casiraghi, M. Lazzeri, F. Mauri, S. Piscanec, D. Jiang, K.S. Novoselov, S. Roth, A.K. Geim, Raman spectrum of graphene and graphene layers, Phys. Rev. Lett. 97 (2006) 187401.
[42] G. Sakai, N.S. Baik, N. miura, N. Yamazoe, Gas sensing properties of tin oxide thin film fabricated from hydrothermally treated nanoparticles, Sens. Actuators B 77 (2001) 116–121.
[43] G. Sakai, N. Matsunaga, K. Shimanoe, N. Yamazoe, Theory of gas-diffusion controlled sensitivity for thin film semiconductor gas sensor, Sens. Actuators B 80 (2001) 125–131.
[44] A. Rothschild, Y. Komem, The effect of grain size on the sensitivity of nanocrystalline metal-oxide gas sensors, J. Appl. Phys. 95 (2004) 6374–6380.
[45] C.N. Xu, J. Tamaki, N. Miura, N. Yamazoe, Grain size effects on gas sensitivity of porous SnO_2-based elements, Sens. Actuators B 3 (1991) 147–155.
[46] S. Liu, B. Yu, H. Zhang, T. Fei, T. Zhang, Enhancing NO_2 gas sensing performances at room temperature based on reduced graphene oxide-ZnO nanoparticles hybrids, Sens. Actuators B 202 (2014) 272–278.
[47] A.C. Catto, L.F. da Silva, C. Ribeiro, S. Bernardini, K. Aguir, E. Longo, V.R. Mastelaro, An easy method of preparing ozone gas sensors based on ZnO nanorods, RSC Adv. 5 (2015) 19528–19533.
[48] Y.C. Cheng, T.P. Kaloni, Z.Y. Zhu, U. Schwingenschlögl, Oxidation of graphene in ozone under ultraviolet light, Appl. Phys. Lett. 101 (2012) 073110.
[49] G. Lee, B. Lee, J. Kim, K. Cho, Ozone Adsorption on graphene: ab initio study and experimental validation, J. Phys. Chem. C 113 (2009) 14225–14229.
[50] X.Q. An, J.C. Yu, Y. Wang, Y.M. Hu, X.L. Yu, G.J. Zhang, WO_3 nanorods/graphene nanocomposites for high-efficiency visible-light-driven photocatalysis and NO_2 gas sensing, J. Mater. Chem. 22 (2012) 8525–8531.